A comparative study of Navier-Stokes and Viscous Shock Layer Solutions for a wide range of Reynolds and Mach numbers

S.Müller
Institut für Geometrie und Praktische Mathematik, RWTH Aachen
Templergraben 55, 52056 Aachen, Germany

N.Yamaleev*
Institute of Mathematics, Russian Academy of Sciences
112 Chernyshevskii St., 450000 Ufa, Russia

A.Klomfass†
Lehr- und Forschungsgebiet für Mechanik, RWTH Aachen
Templergraben 64, 52056 Aachen, Germany

December 18, 1995

Abstract

A parametric comparison of solutions of the full Navier-Stokes equations and the full viscous shock layer (FVSL) equations is presented. These equations are both widely used for modelling of steady supersonic viscous gas flows. The time dependent 2D Navier-Stokes equations are solved with a second order explicit shock-capturing ENO scheme with a finite volume approach. To solve 2D FVSL equations the method of global iterations with respect to the streamwise pressure gradient and the shock standoff distance is used. Computed results are compared for a broad range of Reynolds ($10^3 \le Re_\infty \le 10^5$) and Mach ($5 \le M_\infty \le 15$) numbers.

Key Words: Full Navier-Stokes Equations, Full Viscous Shock Layer Equations, Finite Volume Method, Method of Global Iterations

AMS Subject Classification: 76M25, 35Q30

*Supported by the DAAD, grant no. K A95 07202-113, Ref. 325
†Supported by the Graduiertenkolleg *Transport Phenomena in Hypersonic Flows*

List of symbols

ρ	mass density
p	pressure
T	temperature
a	speed of sound
E	total energy per unit mass
H	total enthalpy per unit mass
h	specific enthalpy per unit mass
(x, y)	Cartesian coordinates
(ξ, η)	Body-oriented (surface, normal) coordinates
(u, v)	Cartesian velocity components
(u_t, v_n)	Body-oriented (tangential, normal) velocity components
λ	heat conduction coefficient
μ	dynamic shear viscosity
$\boldsymbol{\tau}$	stress tensor
$\boldsymbol{q}$	heat flux
M	Mach number
R	universal gas constant
Pr	Prandtl number
Re	Reynolds number
R_n	nose radius
c_p	specific heat at constant pressure
c_v	specific heat at constant volume
γ	ratio of specific heats
V_∞	absolute value of free-stream velocity vector

Subscripts

∞	free stream condition
s	post shock condition
w	wall condition

Superscripts

$\tilde{}$	nondimensional quantities

1 Introduction

The prediction of compressible viscous fluid flows is an essential part in the field of re-entry aerodynamics. The problem is characterised by a wide range of the free stream flow parameters which are the Reynolds number and the Mach number if perfect gas flows are considered.

The full Navier-Stokes equations are the most accurate model used to describe viscous gas flows. Up to now this system of equations is discretized by finite volume or finite difference schemes based on shock-capturing techniques. However, the time-dependent approaches to the solution of these equations are very expensive in terms of computer time especially in case of high-Reynolds-number flows, when the boundary layer and bow shock are very thin.

In order to overcome that problem a number of different forms of reduced Navier-Stokes equations have been developed. One of these is the full viscous shock layer (FVSL) system of equations. The steady FVSL equations can be solved by a method based on space-marching iterations. That approach requires much less computational time than the solution of the time dependent Navier-Stokes equations. But it should be emphasised that the FVSL equations can be applied only for calculating supersonic gas flows without streamwise separation. For that reason it is very important to determine the limits of applicability of this system of equations.

The main objective of this paper is to compare the numerical solutions of both sets of equations over a wide range of Reynolds and Mach numbers. The use of two different approaches to the calculation of the bow shock wave namely shock-capturing and shock-fitting techniques, makes this comparison even more general.

The supersonic laminar perfect gas flow past a spherical blunt body nose is used as a test problem. The stagnation streamline quantities, body surface distributions and two dimensional flow fields are compared. The calculations are carried out with three Mach numbers ($M_\infty = 5, 10, 15$) and three Reynolds numbers ($Re_\infty = 10^3, 10^4, 10^5$).

2 Fluid dynamic equations

In the present analysis we compare the 2D full Navier–Stokes equations with the 2D full viscous shock layer equations for the perfect gas model.

2.1 Full Navier–Stokes equations

The physical model of a compressible fluid without external forces is given by the volumetric balance equations for mass, momentum and total energy. This set of equations is given as:

$$\frac{\partial \rho}{\partial t} + \operatorname{div}(\rho \boldsymbol{v}) = 0 \tag{1}$$

$$\frac{\partial \rho \boldsymbol{v}}{\partial t} + \operatorname{div}(\rho \boldsymbol{v} \circ \boldsymbol{v} + p\boldsymbol{E}) - \operatorname{div}(\boldsymbol{\tau}) = \boldsymbol{0} \tag{2}$$

$$\frac{\partial \rho E}{\partial t} + \operatorname{div}(\rho H \boldsymbol{v}) - \operatorname{div}(\boldsymbol{\tau}\boldsymbol{v} - \boldsymbol{q}) = 0 \tag{3}$$

with

$$E = e + \boldsymbol{v}^2/2, \quad H = E + p/\rho. \tag{4}$$

Throughout this paper, we consider an ideal gas, i.e. we assume constant heat capacities and a thermally perfect gas. The pressure is then given as

$$p = \rho e(\gamma - 1) \tag{5}$$

with

$$\gamma = \frac{c_p}{c_v}. \tag{6}$$

The stress tensor and the heat flux are given by

$$\boldsymbol{\tau} = \mu \left\{ \textbf{grad } \boldsymbol{v} + (\textbf{ grad } \boldsymbol{v})^T - \frac{2}{3}(\text{ div } \boldsymbol{v})\boldsymbol{E} \right\}, \tag{7}$$

$$\boldsymbol{q} = -\lambda \textbf{ grad } T. \tag{8}$$

For the calculation of the shear viscosity μ the Sutherland law,

$$\mu = 1.458 \times 10^{-6} \frac{T^{1.5}}{T + 110.4}, \tag{9}$$

is applied. The heat conduction coefficient λ is determined from the Prandtl number which is taken as a constant,

$$\lambda = \frac{\mu c_p}{Pr}. \tag{10}$$

Let us consider the boundary conditions at the wall. The wall pressure is calculated by the momentum equation of the steady Navier-Stokes equations normal to the wall (see [4], p. 316, [5], p. 82) given by

$$\frac{\partial p}{\partial \eta} = \frac{d \mu}{d T} \left(\frac{\partial T}{\partial \xi} \frac{\partial u_t}{\partial \eta} + \frac{4}{3} \frac{\partial T}{\partial \eta} \frac{\partial v_n}{\partial \eta} \right) + \mu(T) \left(\frac{4}{3} \frac{\partial^2 v_n}{\partial^2 \eta} + \frac{1}{3} \frac{\partial^2 u_t}{\partial \xi \, \partial \eta} \right), \tag{11}$$

and the wall temperature is prescribed as a constant.

2.2 Full viscous shock layer equations

It is well known that the supersonic viscous gas flow can be described by the full viscous shock layer (FVSL) equations [6] if no streamwise flow separation occurs. This system of equations can be obtained from the full, steady state Navier-Stokes equations by retaining terms up to the second order in the inverse square root of the Reynolds number in both the viscous and inviscid regions. In other words, in the full Navier-Stokes equations all mixed and second derivatives in the stream wise direction and all viscous terms in the normal momentum equation are neglected. In the axisymmetric case, for a steady flow without body forces and external heat sources, the FVSL equations can be written in a body-oriented coordinate system in nondimensional quantities as

$$\frac{\partial \left(H_2 \tilde{\rho} \tilde{u}_t\right)}{\partial \tilde{\xi}} + \frac{\partial \left(H_1 H_2 \tilde{\rho} \tilde{v}_n\right)}{\partial \tilde{\eta}} = 0, \tag{12}$$

$$\tilde{\rho}\left[D\tilde{u}_t - \frac{\tilde{u}_t\tilde{v}_n}{H_1}\frac{\partial H_1}{\partial \tilde{\eta}}\right] = -\frac{1}{H_1}\frac{\partial \tilde{p}}{\partial \tilde{\xi}} + \frac{1}{H_1^2 H_2 Re_\infty}\frac{\partial}{\partial \tilde{\eta}}\left[H_1^3 H_2 \tilde{\mu}\frac{\partial}{\partial \tilde{\eta}}\left(\frac{\tilde{u}_t}{H_1}\right)\right], \tag{13}$$

$$\tilde{\rho}\left[D\tilde{v}_n - \frac{\tilde{u}_t^2}{H_1}\frac{\partial H_1}{\partial \tilde{\eta}}\right] = -\frac{\partial \tilde{p}}{\partial \tilde{\eta}}, \tag{14}$$

$$\tilde{\rho}D\tilde{H} = \frac{1}{H_1 H_2}\frac{\partial}{\partial \tilde{\eta}}\left(\frac{H_1 H_2 \tilde{\mu}}{Pr Re_\infty}\left[\frac{\partial \tilde{H}}{\partial \tilde{\eta}} + \frac{V_\infty \tilde{u}_t (Pr-1)}{H_\infty}\frac{\partial \tilde{u}_t}{\partial \tilde{\eta}} - \frac{Pr\, \tilde{u}_t^2 V_\infty^2}{H_\infty H_1}\frac{\partial H_1}{\partial \tilde{\eta}}\right]\right) \tag{15}$$

with

$$D = \frac{\tilde{u}_t}{H_1}\frac{\partial}{\partial \tilde{\xi}} + \tilde{v}_n\frac{\partial}{\partial \tilde{\eta}}, \quad \tilde{H} = \tilde{h} + \frac{V_\infty^2}{2H_\infty}(\tilde{u}_t^2 + \tilde{v}_n^2). \tag{16}$$

For the body-oriented coordinate system the metric coefficients H_1, H_2 are given by

$$H_1 = 1 + \tilde{\eta}\kappa(\tilde{\xi}), \quad H_2 = \tilde{r}_w(\tilde{\xi}) + \tilde{\eta}\cos\alpha(\tilde{\xi}), \tag{17}$$

where $\tilde{r}_w$ is the radius measured from the body axis to the body surface, $\tilde{\kappa}$ is the local curvature of the body surface, α is the body surface angle measured from the body axis. For a sphere with radius R_n the coordinates ξ and η are given by

$$\xi = \arctan\left(-\frac{x}{y}\right), \quad \eta = \sqrt{x^2+y^2} - R_n. \tag{18}$$

The physical quantities in (12)-(16) were nondimensionalized as follows: the length quantities by the body nose radius R_n, pressure by $\rho_\infty V_\infty^2$, temperature by $V_\infty^2 R^{-1}$, the remaining quantities are nondimensionalized by their free stream values respectively. The nondimensionalized equation of state reads:

$$\tilde{h} = \frac{\gamma\tilde{p}V_\infty^2}{(\gamma-1)\tilde{\rho}H_\infty}. \tag{19}$$

The viscosity coefficient and the heat flux coefficient are calculated from (9) and (10). The FVSL equations are solved in the region between the body surface and the bow shock wave surface, i.e. within the shock layer.
To close the FVSL equations the following boundary conditions are imposed. The bow shock wave is treated as a discontinuity, across which the Rankine-Hugoniot conditions [7] are applied to determine the flow quantities immediately behind the shock. In body-oriented coordinate system these equations are given as

$$\tilde{v}_{ns} = \tilde{u}_{ts}\tan\beta_s - \tilde{k}_s\frac{\sin\beta}{\cos\beta_s} \tag{20}$$

$$\tilde{p}_s = \frac{1}{\gamma M_\infty^2} + (1-\tilde{k}_s)\sin^2\beta \tag{21}$$

$$\tilde{u}_{ns} = \cos\beta\cos\beta_s + \tilde{k}_s\sin\beta\sin\beta_s - \frac{\tilde{\mu}_s}{Re_\infty}\frac{\cos\beta_s}{\sin\beta}\left[\frac{\partial \tilde{u}_t}{\partial \tilde{\eta}} - \frac{\tilde{u}_t}{H_1}\frac{\partial H_1}{\partial \tilde{\eta}}\right]_s \tag{22}$$

$$\tilde{H}_s = 1 - \frac{\tilde{\mu}_s}{Re_\infty Pr}\frac{\cos\beta_s}{\sin\beta}\left[\frac{\partial \tilde{H}}{\partial \tilde{\eta}} + \frac{(Pr-1)V_\infty^2\tilde{u}_t}{H_\infty}\frac{\partial \tilde{u}_t}{\partial \tilde{\eta}} - \frac{\tilde{u}_t^2 Pr V_\infty^2}{H_\infty H_1}\frac{\partial H_1}{\partial \tilde{\eta}}\right]_s \tag{23}$$

with

$$\tan \beta_s = \frac{1}{H_{1s}} \frac{\partial \tilde{\eta}_s}{\partial \tilde{\xi}}, \quad \tilde{k}_s = \frac{1}{\tilde{\rho}_s}, \quad \beta = \beta_s + \alpha \tag{24}$$

where β_s is the angle between the bow shock and body surfaces, $\tilde{\eta}_s$ is the shock standoff distance measured from the body surface. Note that the shock slip due to the molecular fluxes is included in the above relations.

On the body surface the conditions of vanishing slip and vanishing mass transfer are imposed; the wall temperature is prescribed, i.e.

$$\tilde{u}_t(\tilde{\xi}, 0) = \tilde{v}_n(\tilde{\xi}, 0) = 0, \quad \tilde{T}(\tilde{\xi}, 0) = \tilde{T}_w. \tag{25}$$

3 Numerical Methods

To solve the systems (1) - (3) and (12) - (15) two different techniques are applied. In the following we will give a short summary. Details can be looked up in the cited references.

3.1 Finite Volume Method

The system of partial differential equations (PDE's) can be written formally as

$$\frac{\partial \mathbf{u}}{\partial t} + \frac{\partial \mathbf{F}(\mathbf{u})}{\partial x} + \frac{\partial \mathbf{G}(\mathbf{u})}{\partial y} = \mathbf{0} \tag{26}$$

with

$$\begin{aligned}
\mathbf{u} &= (\rho, \rho u, \rho v, \rho E)\,, \\
\mathbf{F}_I(\mathbf{u}) &= \left(\rho u, \rho u^2 + p, \rho u v, \rho u H\right), \\
\mathbf{G}_I(\mathbf{u}) &= \left(\rho v, \rho u v, \rho v^2 + p, \rho v H\right), \\
\mathbf{F}_V(\mathbf{u}) &= (0, \tau_{11}, \tau_{21}, \tau_{11} u + \tau_{12} v - q_1)\,, \\
\mathbf{G}_V(\mathbf{u}) &= (0, \tau_{12}, \tau_{22}, \tau_{21} u + \tau_{22} v - q_2)\,, \\
\mathbf{F}(\mathbf{u}) &= \mathbf{F}_I(\mathbf{u}) - \mathbf{F}_V(\mathbf{u}), \\
\mathbf{G}(\mathbf{u}) &= \mathbf{G}_I(\mathbf{u}) - \mathbf{G}_V(\mathbf{u}).
\end{aligned} \tag{27}$$

For the discretization of (26) an explicit shock-capturing scheme is applied via a finite volume approach, where (26) is integrated over a space-time continuum. The spatial integration is transformed into the integration along the cell's boundary using Gauss' theorem. Hence, the rate of change of the average values of the conservative quantities is equal to the difference of the fluxes across the boundary.

The spatial solution domain is discretized by a body fitted orthogonal grid, composed by regular quadrilateral cells. The dimensional splitting technique is applied to calculate the fluxes about each cell boundary as a quasi-onedimensional problem. It is assumed that the conservation quantities are constant along each part of the boundary in the considered time interval. Hence, the fluxes through the cell boundaries are assumed to be constant too and are to be evaluated at the midpoints of the cell boundaries only. For this task a 1D-ENO scheme [1] is applied in the two space directions simultaneously. The basics of the one-dimensional scheme are the following:

A one-dimensional scalar reconstruction approximates a scalar function from given averages at discrete points as piece-wise continuous functions. These discrete average values correspond to the approximate values of the conservation quantities. It has to be guaranteed that the averages of the reconstruction at the discrete points are identical with the given averages. This demand is the discrete analogon to the principle of conservation valid for the conservation variables. In the literature, two different methods can be found which were analysed for the case of a perfect gas [1]. Following [1] the so-called RP-Reconstruction has been chosen. This scalar one-dimensional technique is based on the interpolation of the primitive function given by its averages at discrete points. The knots are chosen due to the smallest absolute values of the derivatives approximated by divided differences. Then, the derivation of the interpolation polynomial provides the continuous approximation of the function being reconstructed. The extension from the scalar case to a system is done by applying the scalar technique to components. This technique is applied to every discretization interval. By this way the reconstruction of the conservation quantities over the whole discretization domain is made up from the local reconstruction polynomials. However, the global reconstruction is not necessarily continuous at the local interfaces, since the limiting values from different cell sides are different, generally computing the fluxes one of both has to be selected following physical principles. This is obeyed in the Riemann solver.

The extension of the one-dimensional scheme to two space dimensions is realised by connecting the midpoints of two opposite cell edges. By this a group of one parametric curves is constructed and to each of them the 1D-ENO scheme is applied. At every cell edge midpoint a Riemann problem is to be solved in order to calculate the fluxes normal to the cell boundary. Since the fluxes in eq. (26) consist of inviscid and viscous parts, the solution of the Riemann problem is evaluated for the Eulerian part of the partial differential equations assuming the gas locally as frozen. In order to evaluate the viscous fluxes the related derivatives of velocity, temperature, mass fraction etc. are discretized by central differences. The conservation quantities are averaged combining the values of the adjacent cells.

The main computational work is to be done in the construction and evaluation of the reconstruction polynomials and in solving the Riemann problems.

Here, Roe's approximative Riemann solver is used in the presentation of Liu and Vinokur [2]. The disadvantage of this solver is its numerical instability for high Mach numbers. Possible corrections are given in [3].

For more details of the two-dimensional algorithm see [5].

The algorithm was first implemented for two cartesian space variables. In order to apply the algorithm also for rotational symmetric flow the 3D-Navier-Stokes equations have been transformed to cylindrical coordinates. Assuming rotational symmetry and thus vanishing circumferential velocity the equations differ from eq. (26) only by an additional source term $\mathbf{R}(\mathbf{u})/y$:

$$\frac{\partial\, \mathbf{u}(x,y,t)}{\partial\, t} + \frac{\partial\, \mathbf{F}(\mathbf{u}(x,y,t))}{\partial\, x} + \frac{\partial\, \mathbf{G}(\mathbf{u}(x,y,t))}{\partial\, y} = -\mathbf{R}(\mathbf{u}(x,y,t))/y \tag{28}$$

with

$$\boldsymbol{R}^I = \begin{pmatrix} \rho v \\ \rho uv \\ \rho vv \\ \rho Hv \end{pmatrix}, \; \boldsymbol{R}^V = \begin{pmatrix} 0 \\ -\mu(\frac{\partial v}{\partial x} + \frac{\partial u}{\partial y}) + \frac{2}{3}\frac{\partial uv}{\partial x} \\ -\left(2\mu\frac{\partial v/y}{\partial y} - \frac{2}{3}\frac{\partial \mu v/y}{\partial y}\right) y \\ \tau_{xy}u + \tau_{yy}v - q_y + \frac{2}{3}\left(\frac{\partial \mu uv}{\partial x} + \frac{\partial \mu vv}{\partial y}\right) \end{pmatrix} \tag{29}$$

$$\mathbf{R} = \mathbf{R}^I - \mathbf{R}^V. \tag{30}$$

Of course, for the source term a discretization must be chosen which avoids possible numerical trouble caused by the $1/y$-term at the x-axis. This is possible since the singularity has no physical nature in this case.

3.2 Method of global iterations

The efficient iterative space-marching method proposed in [6] and improved in [8] is used to solve the FVSL equations. It is well known that these equations are elliptic in the subsonic regions where $\tilde{u}_t < \tilde{a}$. These regions always exist near a body surface, since no slip conditions are imposed on the wall. It means that it is impossible to find the solution of the FVSL equations for one marching sweep on the computational domain.
To take into account the elliptic properties of the FVSL equations the method of global iterations are used. The global iterations are carried out with respect to the streamwise pressure gradient component $\partial\tilde{p}/\partial\tilde{\xi}$ and the first derivative of the shock standoff distance $\partial\tilde{\eta}_s/\partial\tilde{\xi}$. The term $\partial\tilde{p}/\partial\tilde{\xi}$ in $\tilde{\xi}$ - momentum equation (13) at i-th global iteration is represented as

$$\frac{\partial \tilde{p}}{\partial \tilde{\xi}} = \omega\left(\frac{\partial \tilde{p}}{\partial \tilde{\xi}}\right)^i + (1-\omega)\left(\frac{\partial \tilde{p}}{\partial \tilde{\xi}}\right)^{i-1}. \tag{31}$$

The transformed FVSL equations become parabolic and the Cauchy problem is well-posed as an initial value problem with respect to the coordinate $\tilde{\xi}$ if

$$0 \le \omega \le \frac{\tilde{u}_t^2}{\tilde{a}^2}, \;\; \tilde{u}_t \ge 0. \tag{32}$$

These equations can be solved by using a space-marching method on coordinate $\tilde{\xi}$. To find the solution of the original FVSL equations this procedure should be repeated iteratively. To account for the disturbance propagation in the upstream direction, central differences are used for the approximation of the terms $(\partial\tilde{p}/\partial\tilde{\xi})^{i-1}$ and $(\partial\tilde{\eta}_s/\partial\tilde{\xi})^{i-1}$.
The calculation of the current i-th global iteration is carried out using the quantities $(\tilde{p})^{i-1}$ and $(\tilde{\eta}_s)^{i-1}$ obtained from the previous global iteration. For the next global iteration the pressure distribution and the shock standoff distance are calculated from:

$$\tilde{p} = \tau_p\tilde{p}^i + (1-\tau_p)\tilde{p}^{i-1} \tag{33}$$

$$\tilde{\eta}_s = \tau_s\tilde{\eta}_s^i + (1-\tau_s)\tilde{\eta}_s^{i-1}, \tag{34}$$

where τ_p and τ_s are the relaxation parameters. From the stability condition of the iteration process for both the pressure and the shock standoff distance, the following restrictions are derived:

$$0 < \tau_p < 2, \;\; 0 < \tau_s < \frac{\Delta\tilde{\xi}}{\tilde{\eta}_s} \tag{35}$$

The global iterations on the shock standoff distance are carried out only for the fore-body part of the flow, since in this case the subsonic region is located from the body surface up to the bow shock. However, for the downstream part of the flow the shock standoff distance can be calculated by a marching method without iterations, because the subsonic region is a thin zone located near the body surface. To determine the bow shock angle, which is required for the calculation of the shock standoff distance, the Rankine-Hugoniot boundary relation for the normal velocity $\tilde{v_{ns}}$ (20) is applied [9]. This relation is not used in calculating the current global iteration and can therefore be used for the determination of the shock location for the next global iteration.
To solve the differential set of equations at each global iteration the following implicit finite difference scheme is applied. The derivatives in the streamwise direction are approximated by using the 2nd order implicit finite difference scheme proposed in [11]. 4th order finite difference scheme [10] is used to approximate the normal derivatives.
For the calculation of flows with large Reynolds numbers, a grid adaption in normal direction $\tilde{\eta}$ is applied. The grid step size at each point is chosen in accordance with the values of $\partial\tilde{u}_t/\partial\tilde{\eta}$ and $\partial^2\tilde{u}_t/\partial\tilde{\eta}^2$, [12]. This approach allows one to calculate the flow field over a wide range of Reynolds numbers ($10^2 \leq Re_\infty \leq 10^7$) with high accuracy by using a moderate number of grid nodes.

4 Results and Comparisons

The main objective of the present paper is the validation of the FVSL solutions in comparison with the full Navier-Stokes solutions. To this purpose several test calculations were carried out for a wide range of Mach numbers ($M_\infty = 5, 10, 15$) and Reynolds numbers ($Re_\infty = 10^3, 10^4, 10^5$). The free stream conditions are given in Tab. 1. The free stream temperature was chosen as $T_\infty = 212$ K for all calculations.

		15 - 3	15 - 4	15 - 5	10 - 3	10 - 4	10 - 5	5 - 3	5 - 4	5 - 5
Ma_∞		15	15	15	10	10	10	5	5	5
Re_∞		10^3	10^4	10^5	10^3	10^4	10^5	10^3	10^4	10^5
p_∞	Pa	1.277	12.77	127.7	1.916	19.16	191.6	3.832	38.32	383.2
v_∞	m/s	4393	4393.11	4393	2928	2928	2928	1464	1464	1464

Table 1: Free stream conditions

As a test case the flow of perfect gas about a hemisphere with nose radius $R_n = 0.1524$ m is considered. The wall was assumed to be non-adiabatic. To this purpose the wall temperature was prescribed by $T_w = 1500$ K. In the following the calculated stagnation streamline conditions, the body surface distributions and the two dimensional flow fields are compared.
The stagnation streamline density and velocity compare very well. Therefore, they are not presented here. Certain differences can be seen in quantities like temperature, pressure, etc. Qualitatively similar deviations are found throughout all test cases. As an example, the temperature is presented in Fig. 1, 2 and 3 for the different Mach and Reynolds numbers. The difference between FVSL and NS is about 5% in the worst case for all

test cases. The shock standoff distance as well as the boundary layer thickness is in good agreement for $Re_\infty = 10^4, 10^5$ independent of the Mach number. For the low Reynoldes number $Re_\infty = 10^3$ the shock is very smeared and cannot be described accurately by a discontinuity any longer. Due to the shock fitting technique this region can not be resolved by the FVSL approach (see chap. 2.2). However, there is only a small influence on the post shock conditions. This fact can be explained by using the generalised form of the Rankine-Hugoniot conditions (20) - (23) for the calculation of the post shock quantities. In the boundary layer a different temperature gradient is found in the Navier-Stokes and the FVSL solutions, see Fig. 1, 2 and 3. This has an essential influence on the wall heat flux. The latter is presented in Fig. 4, 5 and 6. We notice that for increasing Reynolds number the differences between FVSL and NS solutions are diminishing. For the stagnation point heat flux absolute values are summarised in Tab. 2.
For the high Reynolds number $Re_\infty = 10^5$ we got moderate differences of at most 4% whereas the differences are increasing with decreasing Reynolds number. This seems to indicate that for low Reynolds numbers there is a certain error arising from the simplifying assumptions in the derivation of the FVSL equations. In this case the boundary layer can be well resolved by an explicit finite volume scheme. It becomes more difficult with increasing Reynolds numbers. On the other hand we know from numerous calculations for the finite volume scheme that the wall heat flux is a very sensitive quantity and its value depends seriously on the computational grid, especially in the number of points normal to the wall and the aspect ratio of the cells in the boundary layer. It is also influenced by the numerical dissipation inherent in the second order finite volume scheme. This scheme applied to the calculation of the Navier-Stokes equations allows one to determine the heat flux only with the first order of approximation, because the heat flux is proportional to the first derivative of the temperature. Moreover, we know from earlier investigations for inviscid stagnation point calculations that the second order scheme results in an error of about 1% near the wall for the total enthalpy from the free stream value (see [5], chap. 7.4). The method of global iterations (see chap. 2.2) is based on a fourth order finite difference scheme and uses an adaptive grid approach. That results in small numerical dissipation. Furthermore, it means that we need a much finer grid for the finite volume scheme to get the same asymptotic as for the method of global iterations.
For comparison, the stagnation point heat flux has furthermore been calculated from the dimensionally reduced Navier-Stokes equations (DRNSE). For details about this approach see [13, 14]. The usage of DRNSE allows a very high resolution of the stagnation streamline. From Tab. 2 we see that the difference to the FVSL results is much more moderate. The deviation is about 2% for the low Reynolds number and increases up to 5% for the high Reynolds number.

	15 - 3	15 - 4	15 - 5	10 - 3	10 - 4	10 - 5	5 - 3	5 - 4	5 - 5
FVSL	170450	505780	1564400	46680	140260	436940	2249	6898	21650
NS	136690	439160	1565200	38202	120350	453210	1389	5072	21373
DRNSE	174400	491700	1485000	47630	136100	415100	2192	6655	20650

Table 2: Stagnation point heat flux [W/m^2]

It should be remarked that the pressure distribution is hardly influenced by viscosity

	15 - 3	15 - 4	15 - 5	10 - 3	10 - 4	10 - 5	5 - 3	5 - 4	5 - 5
FVSL	373	3710	37072	248	2477	24763	125	1251	12514
NS	383	3846	38399	257	2564	25671	129	1299	12947
DRNSE	369	3723	37084	254	2483	24769	127	1252	12508

Table 3: Stagnation point pressure [Pa]

effects and heat conduction. As FVSL and Navier-Stokes equations differ only in the viscous terms it can be concluded that the results regarding the pressure distribution should be close to each other. As Fig. 4, 5 and 6 and Tab. 3 reveal there are however clear deviations between the results. This may be attributed to the low streamwise resolution and in the FVSL calculation.

Finally, we want to discuss the two dimensional flow fields. To this objective the pressure distribution is shown in Fig. 7, 8 and 9 for $M_\infty = 15$ and the respective Reynolds numbers. As we have already seen from the wall pressure, there is a maximal difference in the neighbourhood of the stagnation streamline that is diminishing downstream. The shock standoff distance is in good agreement in the entire flow field.

To obtain the steady state solution of the FVSL equations about 10 global iterations on the body nose part and about 2-3 iterations on the downstream part of the flow field are required. The calculation time remains virtually unchanged for a wide range of Mach numbers ($M_\infty = 5, 10, 15$) and Reynolds numbers ($Re_\infty = 10^3, 10^4, 10^5$). The typical computational time in a case of sphere for the grid 35×40 was about 20 sec on a SGI IRIS work station with a R8000 processor.

In contrast to the method of global iterations the explicit finite volume scheme requires several CPU hours. But it should be stressed that the FVSL equations can only be applied for non-separated supersonic flow fields, while solutions of the Navier-Stokes equations exist also for complex flow fields.

5 Conclusion

A comparative study of the full Navier-Stokes equations and the FVSL equations has been made for a wide range of Mach numbers and Reynolds numbers for perfect gas. The comparisons show that the results are in good agreement for all main flow quantities except for the wall heat flux in the case of low and moderate Reynolds numbers.

Figures

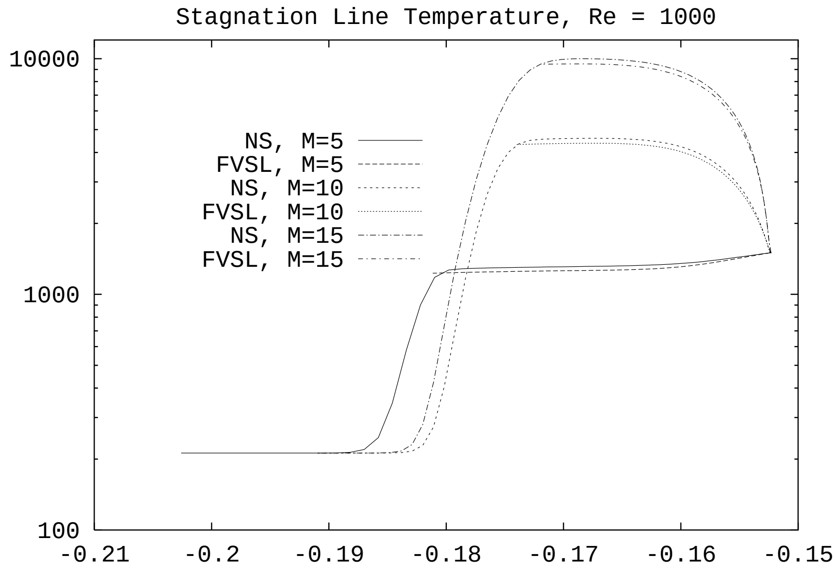

Figure 1:

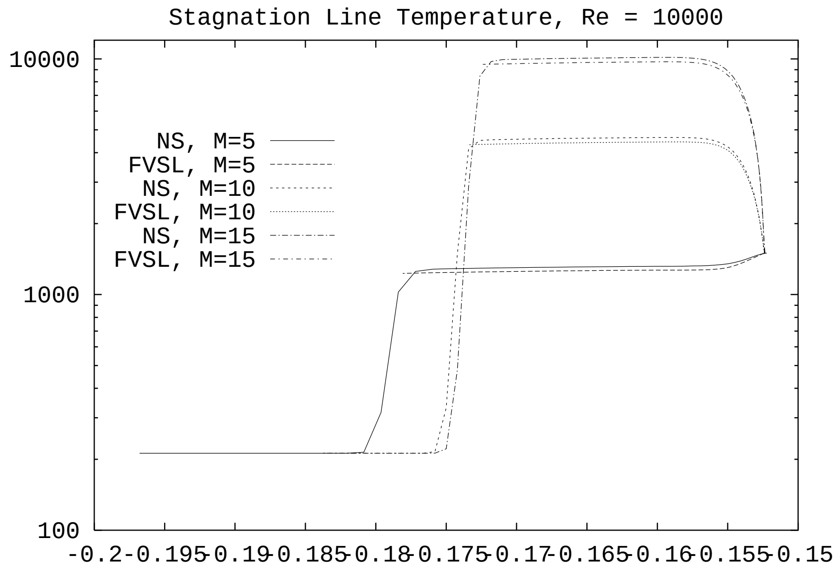

Figure 2:

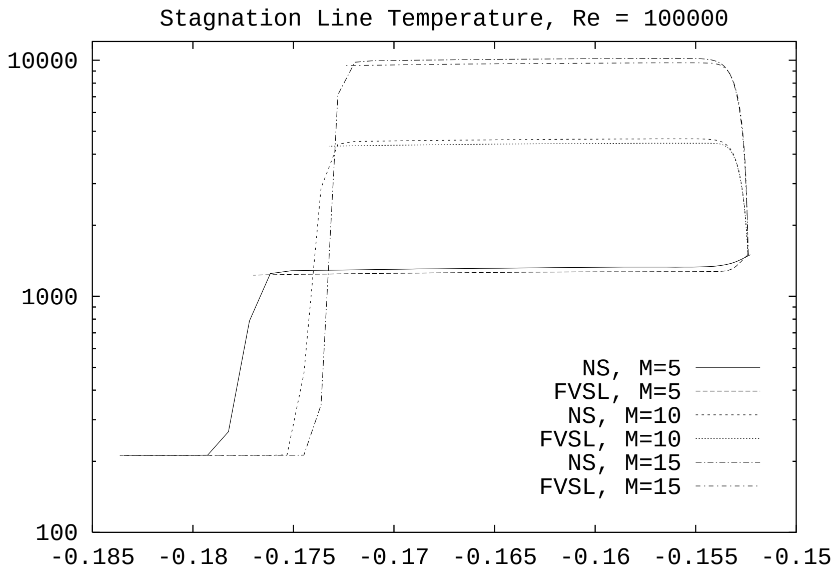

Figure 3:

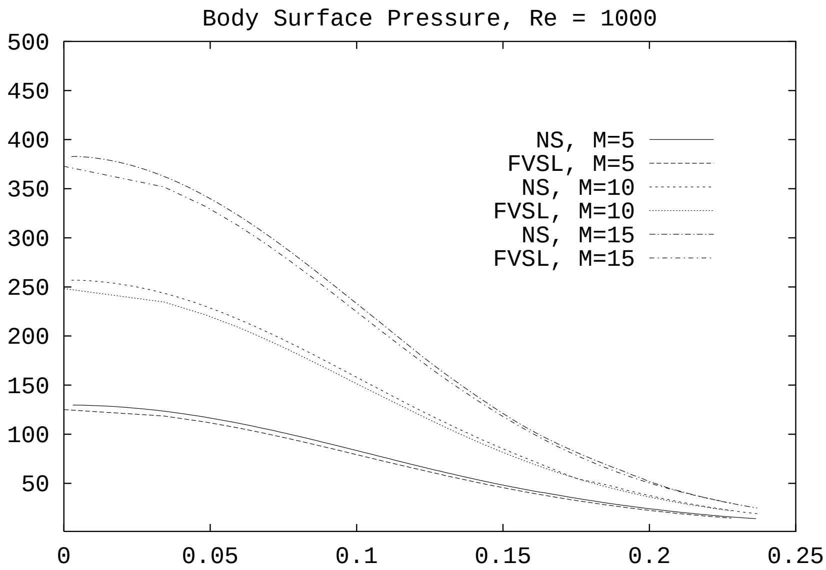

Figure 4:

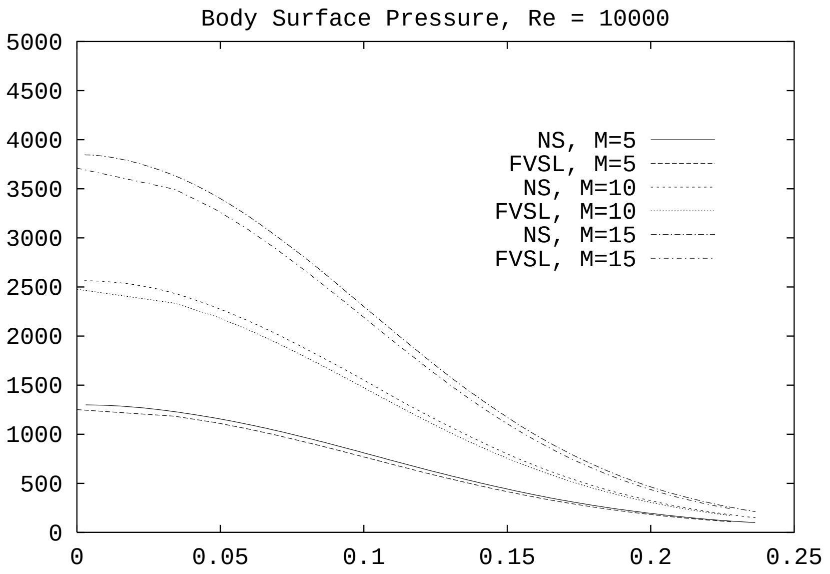

Figure 5:

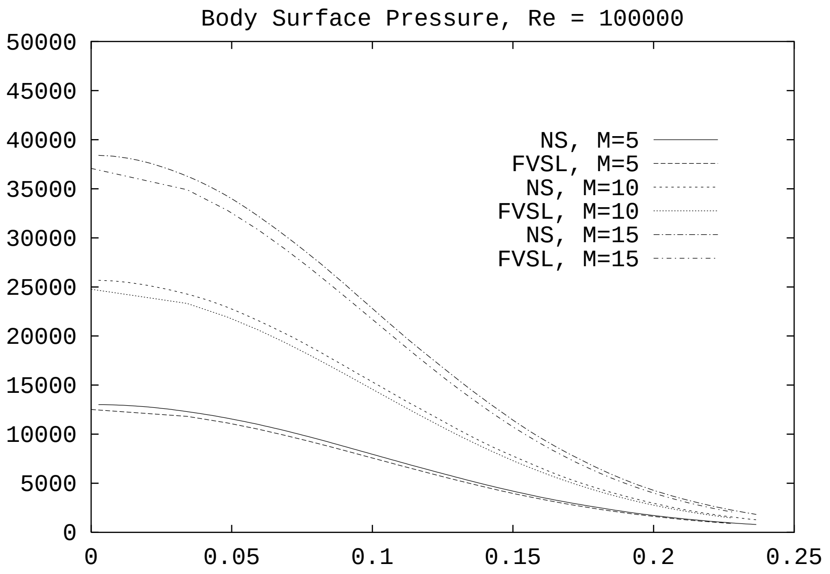

Figure 6:

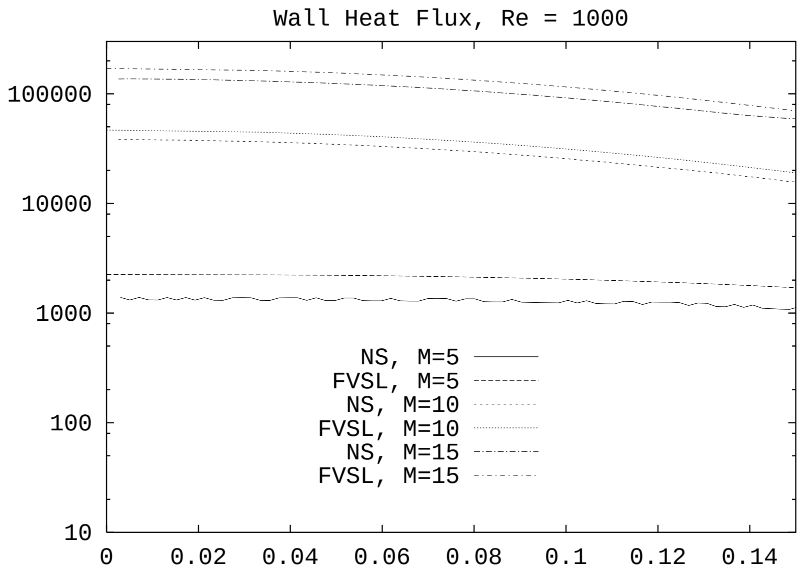

Figure 7:

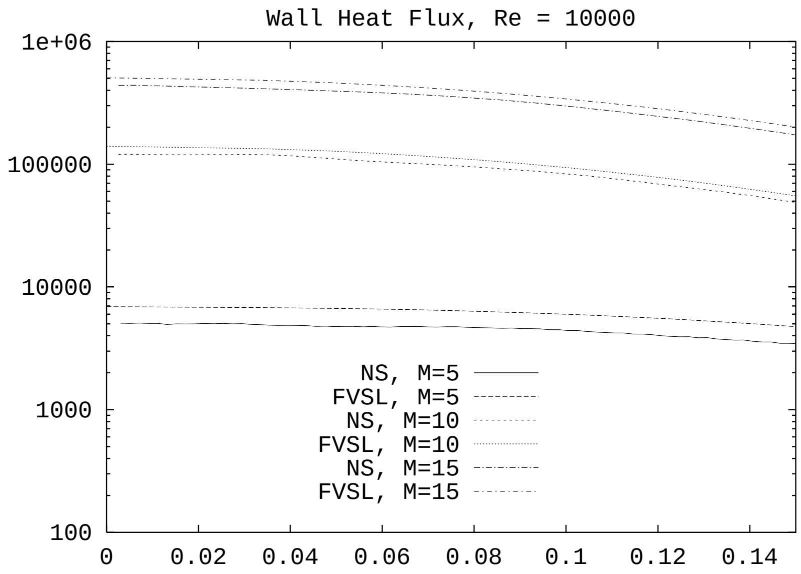

Figure 8:

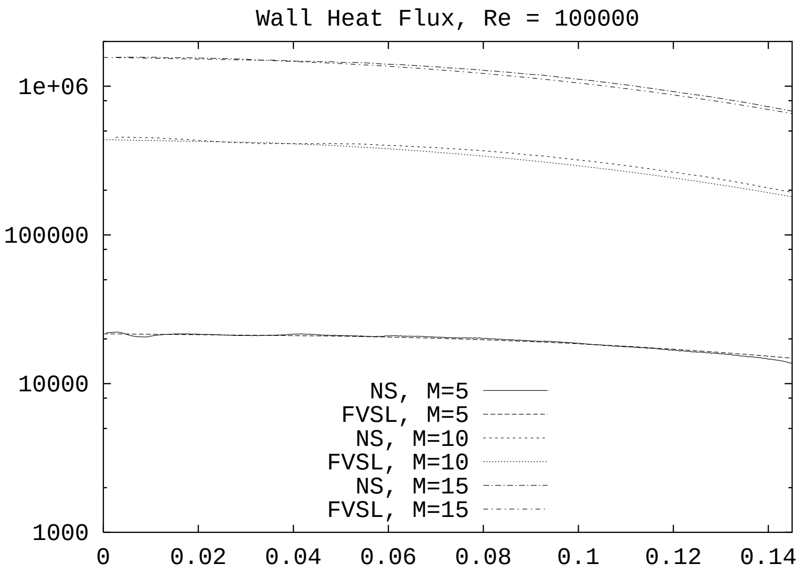

Figure 9:

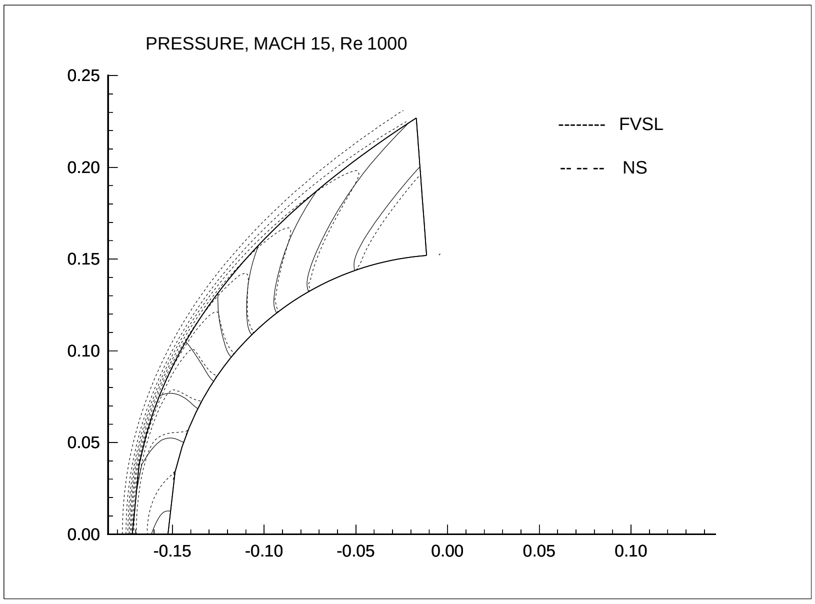

Figure 10:

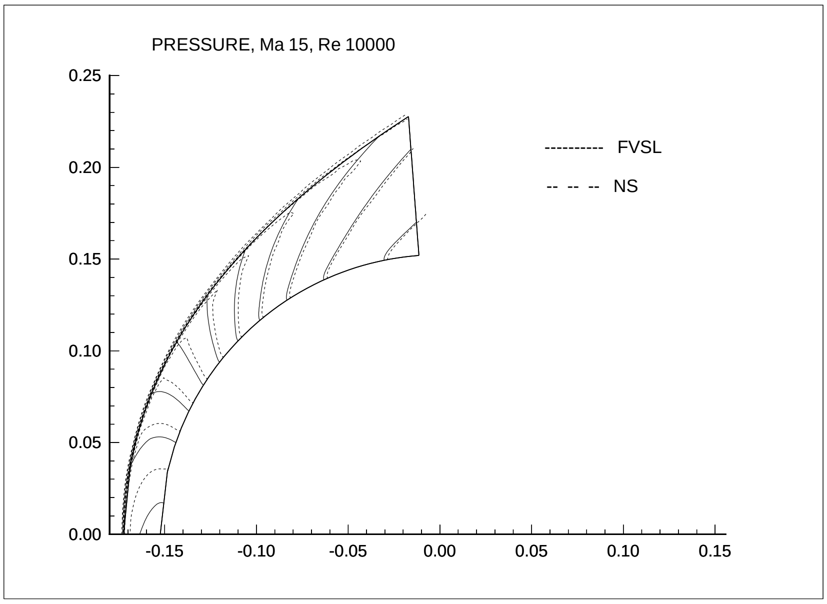

Figure 11:

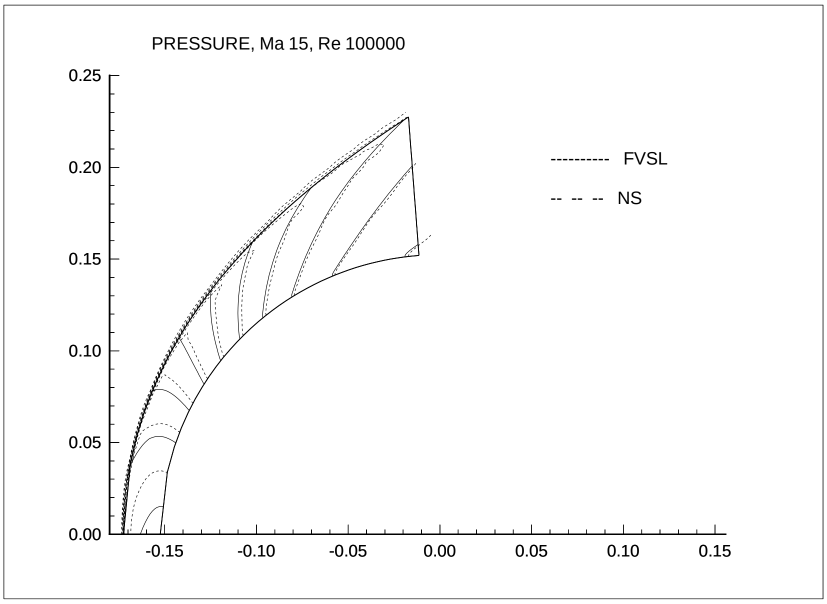

Figure 12:

References

[1] Chakravarthy S.R., Engquist B., Harten A., Osher S., *"Uniformly High Order Accurate Essentially Non-Oscillatory Schemes III"*, J. Comp. Phys., Vol. 71, 1987, pp. 231 - 303

[2] Liu Y. , Vinokur M. , *"Nonequilibrium Flow Computations I. An Analysis of Numerical Formulations of Conservation Laws"*, J. Comp. Phys., Vol. 83, 1989, pp. 373 - 397

[3] Yee, H. C., *"A Class of High-Resolution Explicit and Implicit Shock-Capturing Methods"*, VKI-Lecture Series 04-1989

[4] Peyret, R., Taylor, Th. D., *"Computational Methods for Fluid Flow"*, Berlin, Heidelberg, New York: Springer Verlag 1982

[5] Müller S., *"Extension of ENO schemes to two space dimensions and application to hypersonic stagnation point problems"*, PhD thesis, RWTH Aachen 1993, Verlag Shaker, Aachen (In German)

[6] Davis R.T., *"Numerical solution of the hypersonic viscous shock layer equations"*, AIAA J., Vol. 8, No. 5, 1970

[7] Sedov L.I., *"Mechanics of Continua"*, Vol.1, Nauka, Moscow, 1983, (In Russian)

[8] Lin A., Rubin S.G. *"Three-dimensional supersonic viscous flow over cone at incidence"*, AIAA Paper, No.81-192, 1981

[9] Tirskii G.A., Utyuzhnikov S.V., Yamaleev N.K., *"Efficient numerical method for simulation of supersonic viscous flow past a blunted body at a small angle of attack"*, J. Computers and Fluids, Vol. 23, No. 1, 1994, pp.103-114

[10] Petukhov I.V., *"Numerical calculation of two-dimensional flows with boundary layers"*, In Trans. on Numerical Methods for Solution of differential and Integral Equations, Nauka, Moscow, 1964, pp.304-325, (In Russian)

[11] Richardson L.F., *"The approximate arithmetical solution by finite differences of physical problems involving differential equations, with applications to the stress in a machinery dam"*, Phil. Trans. R. Soc. Lond., Vol. A210, 1910

[12] Dwyer H.A., *"Grid adaption for problems in fluid dynamics"*, AIAA J., Vol. 22, No. 12, 1984

[13] Klomfass A., Müller S., Ballmann J., *"Analysis of Non-Equilibrium, Hypersonic Blunt Body Flow with the Local Similarity Method"*, in: Proc. Int. Symposium on Shock waves, Passadena, USA, 1995

[14] Klomfass A., Müller S., *"Calculation of stagnation streamline quantities in hypersonic blunt body flows"*, Internal Report No. 121 , Institut für Geometrie und Praktische Mathematik, RWTH Aachen, 1995